Available online at www.sciencedirect.com
SCIENCE DIRECT®
Journal of Marine Systems 38 (2003) 205–219
JOURNAL OF MARINE SYSTEMS
www.elsevier.com/locate/jmarsys

Seasonal and wind-induced variability of Sea Surface Temperature patterns in the Gulf of Cádiz

J.M. Vargas*, J. García-Lafuente, J. Delgado, F. Criado

Departamento de Física Aplicada II, Universidad de Málaga, Málaga, Spain

Received 2 February 2001; accepted 12 August 2002

Abstract

The evolution of thermal structures in the Gulf of Cádiz is analysed with a set of 325 weekly composite Sea Surface Temperature (SST) images derived from NOAA–AVHRR sensor, and covering a time span of 7 years, from 1993 to 1999. A spatial Empirical Orthogonal Function (EOF) analysis has been performed in order to identify the main SST spatial patterns. The first EOF mode explains 60% of the temperature variance of the images, and shows a quasi-permanently warmer than the mean region in the southern part of the area of study. The second mode (13% of variance), has a strong temporal variability, and is the main responsible for the cooling and warming of the shelf waters in southwestern Iberia. These two modes explain together most of the seasonal variability of SST over the basin, particularly the variation and strength of the upwelling area located southeast of Portugal. The third mode explains 6% of variance and is well correlated with the local zonal wind. Two wind-induced upwelling can be clearly identified in this mode. The first one, located at the southwestern end of the Strait of Gibraltar, takes place during easterlies events. The second one, related to westerlies, is located to the east of Cape Santa María, and is associated with a southeastward transport of cold surface waters from that Cape.
© 2002 Elsevier Science B.V. All rights reserved.

Keywords: Thermal satellite imagery; Sea Surface Temperature; Northeastern Atlantic; Gulf of Cádiz; Seasonal variability; Spatial variance; Wind stress

1. Introduction

The Gulf of Cadiz is the area that connects the open North Atlantic ocean with the Strait of Gibraltar. Its northern and eastern boundaries are well defined by the Iberian Peninsula and the Atlantic coast of Morocco (Fig. 1) but its western and southern limits are open boundaries that would be defined by imaginary lines running along some accepted parallel and meridian. This means that it is fully connected to the open ocean and, therefore, influenced by the oceanographic processes taking place there.

The surface circulation in the Gulf of Cádiz must be considered in relation to the Norheastern Atlantic circulation. Recent numerical models (Johnson and Stevens, 2000) indicate that the Azores current, a minor branch of the Gulf Stream in the North Atlantic ocean, has its ultimate cause in the outflow of Mediterranean water that entrains surface water to the west. This mechanism leads to a sinking of surface Atlantic flow and triggers the Azores current. The maps of the

* Corresponding author. Tel.: +34-952-132849; fax: +34-952-131450.
E-mail address: jmvargas@ctima.uma.es (J.M. Vargas).

0924-7963/02/$ - see front matter © 2002 Elsevier Science B.V. All rights reserved.
PII: S0924-7963(02)00240-3

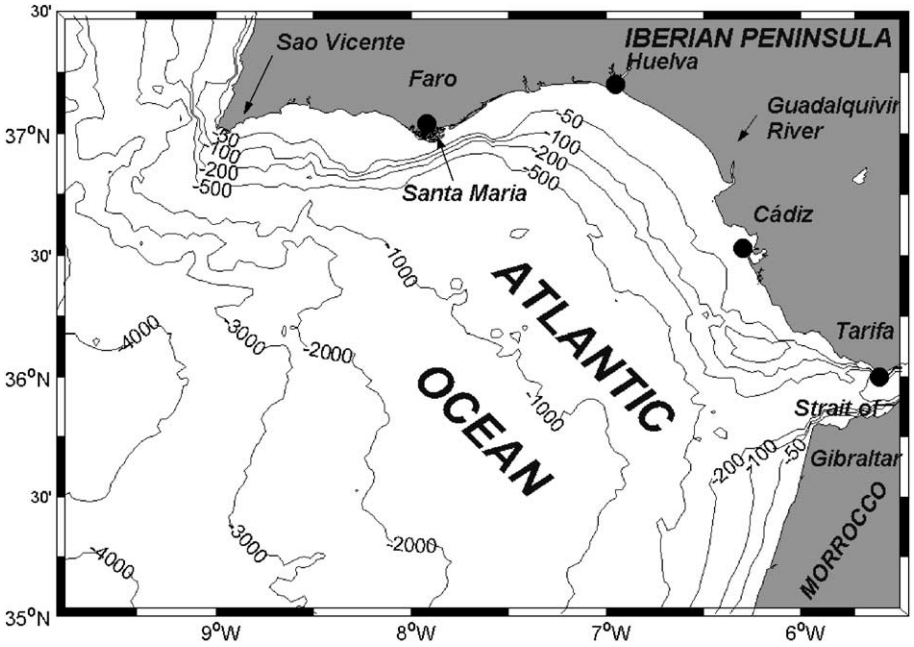

Fig. 1. Map of the area of study, showing the locations and topographic features mentioned in the text.

level of 30 m depth in the above mentioned model show that this current is a meandering jet with a meander length scale of about 300 km. that flows towards the east. The surface circulation in the Gulf of Cadiz can be regarded as the last meander of this jet that, at the same time, feeds the Atlantic inflow through the Strait of Gibraltar into the Mediterranean Sea.

Located at the eastern end of the Gulf, the Strait of Gibraltar have been subjected to strong field work and research, both from the pure physical point of view (e.g. Lacombe and Richez, 1982; Candela et al., 1989; Bryden et al., 1994; García-Lafuente et al., 2000, 2002), and also, more recently, with a more interdisciplinary scope (e.g. Echevarría et al., 2002; Reul et al., 2002). Surprisingly, much less effort has been devoted to the circulation in the Gulf itself. Indeed, most of the literature focuses on the deep circulation (e.g. Ochoa and Bray, 1991), which is dominated by the westerly current of high salinity (S>37) Mediterranean water exiting the sea through the Strait. The formation of Mediterranean water eddies (''Meddies'') detached from this deep current has also been extensively studied. Once formed, these Meddies may travel across the Atlantic for several months without significant mixing with the surrounding, less salty water (e.g. Bower et al., 1995; Baringer and Price, 1997; Ambar et al., 1999).

The surface circulation has been primarily described and inferred using satellite thermal imaginery. In a pioneer work, Stevenson (1977), using visible and infrared remote-sensed imaginery acquired during summer 1975, describes a warm–cold–warm frontal structure running in the SE–NW direction offshore the southwestern Spain, approximately between the cities of Cádiz and Huelva. He named it the ''Huelva Front'', after the latter. A similar pattern, at the same location, is reported by Fiúza (1983): an upwelled water plume extending offshore, during an strong upwelling event during Summer 1979. He describes the upwelling system off southwestern Iberian Peninsula, and in particular around S. Vicente Cape, as an extension of the well known upwelling along the western coast of Iberian Peninsula (e.g. Fiúza et al., 1982; also Fiúza, 1983).

Folkard et al. (1997) have studied the thermal patterns of sea surface temperature (SST) of the Gulf of Cádiz, Strait of Gibraltar and western part of the Alborán Sea using week-long sequences of SST images (derived from NOAA–AVHRR sensor data). They observe a great spatio-temporal variability, which is

particularly noticeable off the southwestern Spanish coastal zone. Their most interesting result is the identification, at least for the summer season, of a clear bimodality in the SST patterns. They also find that the temporal evolution of these patterns is significantly correlated to the zonal wind in the region. One of the patterns is related to westerlies, and is characterized by an extension to the east of the upwelling region around S. Vicente Cape. Simultaneously, they observe a warm water signature travelling to the southeast from the Santa María Cape region to the Strait of Gibraltar. The other pattern, related to easterlies, shows the S. Vicente upwelling restricted to the west, and the shelf off southern Portugal covered by relatively warm waters. Another upwelling area is also evident at the southwest of the Strait of Gibraltar that, subsequently, extends to the west filling a larger area. Finally, they suggest that these wind-induced fluctuations are present all the year round, though their dataset does not allow for a definitive conclusion.

Field work has been carried out in the area by the The Instituto Español de Oceanografía (Spanish Institute of Oceanography, IEO). Summer hydrographic surveys have been carried out during 1995 and 1997 in the continental shelf and slope of the Gulf (Rubín et al., 1999; García et al., in preparation). A region of coastal warm water was found in July 1995 in front of the mouth of Guadalquivir River. However, during the July 1997 survey this warm pool was not found, what suggests an interannual variability feature.

The main surface pattern in the Gulf of Cádiz can be summarize as follows. There are pieces of evidence, both from SST and hydrographic data, on the existence of anticyclonic circulation of warm waters in the central and southern part of the Gulf. A quasi-permanent upwelling area exists around Cape S. Vincent, as a prolongation of the western Iberian coastal upwelling system. This upwelling is known to enhance during the summer, under the dominant northerly winds along the western coast of Portugal (Fiúza et al., 1982). When prevailing winds in the Gulf are from the west, a minor upwelling area is found to the east of Cape Santa María. Strong westerlies force cold surface waters around Cape S. Vicente travel east along the coast. These cold waters eventually join with upwelled waters in Cape Santa María, forming a cold tongue that separates from the coast and flows offshore in the SW direction, towards the Strait of Gibraltar. The "Huelva Front" separates this tongue from the warmer waters of the central part of the Gulf.

Understanding the upwelling and frontal systems at the southwestern coast of the Iberian Peninsula has a great importance, specially looking at its implication for the ecosystems in the region. Given the present uncertainty in both their spatial and temporal variability, a long-term, large-scale description is first needed. In the present work, long-term (almost 7 years) SST data are used to validate and complete the former picture of the surface circulation in the Gulf of Cádiz. The work is organised as follows: Section 2 presents the data and the EOF methodology. In Section 3, the results of the EOF analysis are presented, with special attention to the description of the most important modes. Reconstructed maps of the SST seasonal variation, and of the response of the SST to wind stress are shown in Section 4. Finally, Section 5 summarises the conclusions.

2. Data and methodology

2.1. Data

2.1.1. Satellite images

The satellite images cover the region between 34.7° and 37.2°N in latitude, and between 10° and 5°W in longitude (Fig. 1). This region will be referred to as the 'study region' hereinafter. The dataset consist of $N=356$ weekly composite SST images derived from NOAA–AVHRR infrared sensor data. These images are a value-added product of the German Remote Sensing Data Center (DLR), which can be freely downloaded from its database ISIS in the WWW. The SST-related products are daily, weekly and monthly SST maps based on multiple daily passes. The spatial resolution is 1.1 km. Daily composites are produced from the maximum daily temperature registered at each pixel. Weekly and monthly composite images are produced by simply averaging the temperature of the corresponding daily composites at each pixel. The details of data treatment calibration, navigation and algorithms can be seen at the internet address http://isis.dlr.de/guide/NOAA-AVHRR.html.

The main interest of the present work is to study the seasonal and subinertial variability (i.e. times scales from the order of a few days to the order of a year) of

the sea surface temperature field over the basin, and its relation with the atmospheric forcing. Thus, weekly composite SST images provide a suitable low-pass filter of the field, reducing the influence of temperature structures with time scales of less than a few days.

2.1.2. Wind data

Wind data from the nearby station of Tarifa were obtained from the Instituto Nacional de Meteorología (INM, Spanish Meteorological Institute), for a limited period beginning on January 1995 and ending on December 1998. The sampling interval was 6 h. The data were filtered with a low-pass, 8 order Butterworth filter with cut-off centered at a period of 26 days, in order to have similar smoothness for the wind series as for the modal time series that are described below. The wind series was next subsampled to 1-week intervals, and zonal wind stress was derived in the usual way

$$T(x) = \rho_a C_d \mid V \mid U \tag{1}$$

where $\rho_a = 1.2$ kg m^{-3} is the air density, $C_d = 1.4 \times 10^{-3}$ the non-dimensional drag coefficient, $\mid V \mid$ the wind speed modulus and U the zonal wind component.

2.2. Methodology

As a first step, a visual check of the images was performed, and images with strange temperature patterns (e.g. sharp, rectilinear edges) were rejected.

A different but important issue is the problem of cloud cover. This problem is strongly reduced for weekly composites in comparison to daily images. However, there still exist a number of images in which a considerable percentage of "sea" pixels (defined as those pixels that do not belong to the ground mask) are covered by clouds.

Instead of rejecting all images with clouds, an intermediate solution has been adopted. After some trials, only images with more than 10% of "sea" pixels covered by clouds where rejected. The masking effect of clouds in the non-rejected images was considered small enough to allow the main temperature patterns in those images to be readily identified by eye. To minimise the effect on the image variance of cloud pixels in the selected subset of images, the mean temperature over the rest of "sea" pixels in each image is assigned to the cloud pixels. This way the contribution of these pixels to the variance of each image and to the covariance between images is identically zero. Obviously the resulting images do not represent the real SST field, but the method described tends to reduce the influence of this departure in the images' variance for reasons that will be clarified in the following section.

A total of 31 images, mostly from the winter where rejected, and the number of useful images reduces to $N = 325$. Fig. 2 presents the percentage of cloudy pixels versus image number; circles mark rejected images. More elaborated approaches to EOF analysis of cloudy images and incomplete data can be found in Everson and Sirovich (1995) and Everson et al. (1997).

Prior to further processing, a low-pass filter and subsampling was applied to reduce high frequency noise. The filter form is similar to that proposed by Fang and Hsien (1993).

$$F = \frac{1}{16}\begin{bmatrix} 1 & 2 & 1 \\ 2 & 4 & 2 \\ 1 & 2 & 1 \end{bmatrix} \tag{2}$$

The filter was applied whenever no ground pixels were present within the filter window. In other case, the corresponding subsampled image value was set to zero (digital value for ground). After subsampling, the spatial resolution of the images is 3.3 km.

2.3. Empirical Orthogonal Functions (EOF) analysis

When analysing a large set of SST images, it is of great interest to study the variance associated with temperature fronts, eddies or quasi-permanent features observed in certain regions. It is desirable to separate the mentioned variance into different contributions that correlate with different causes. The method known as "spatial" EOF analysis performs this issue in a quite suitable way for the present study.

EOF analysis is also known by other names, as, for example, Principal Component Analysis. As pointed out by Sirovich and Everson (1992), it is a mathematical procedure that has been rediscovered several times in different disciplines. It was introduced in the Earth sciences by Obukhov (1947) and Lorenz (1956). There are many examples in the literature concerning EOF analysis of SST images. It has been applied to regions

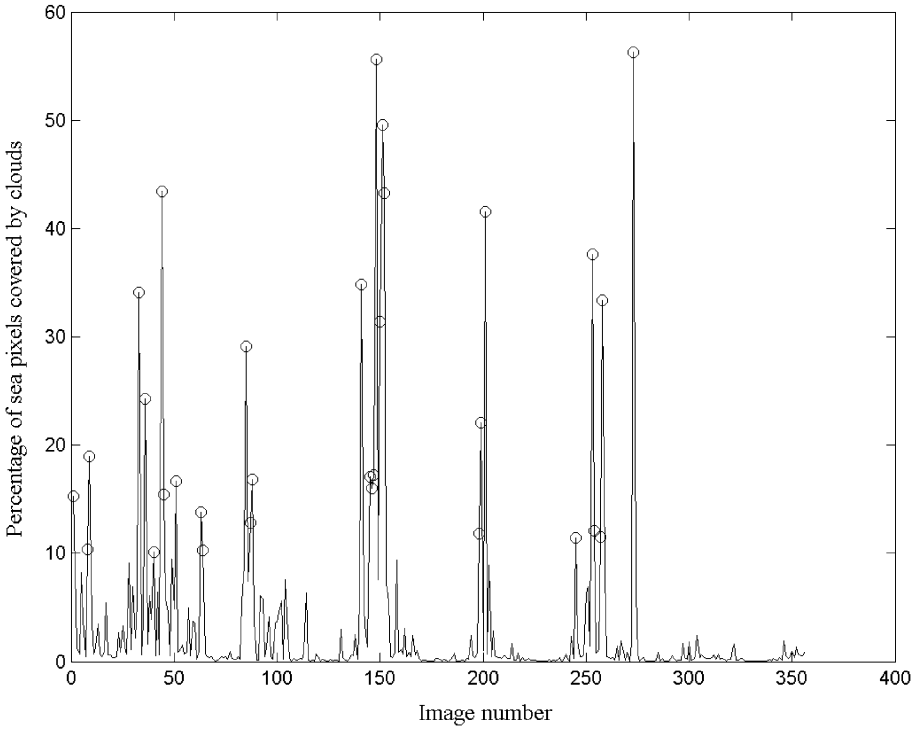

Fig. 2. Percentage of cloudy "'sea" pixels versus image number. Circles mark those images with more than 10% of "sea" pixels covered by clouds.

close to the Gulf of Cádiz, as the Alborán Sea (Parada and Cantón, 1998; Álvarez et al., 2000) or off the African northwestern coast (Hernández-Guerra and Nykjaer, 1997).

The aim of the method is to represent a large set of spatio-temporal data by using a finite and, desirably, reduced set of functions from which mainly of the original information can be easily recovered. In the case of SST images, if the reduced set of these new functions contains a large amount of the variance present in the original dataset, then they may reflect the existence of some stable surface circulation pattern, or the response of the sea surface to some quasi-permanent external forcing mechanisms.

A modification of the standard EOF analysis, called "spatial variance EOF" and first suggested by Lagerloef and Bernstein (1988), will be implemented in this work. Let us consider the spatially demeaned SST

$$T_e(\mathbf{x},t) = T(\mathbf{x},t_m) - \langle T(\mathbf{x},t_m)\rangle \tag{3}$$

where angled brackets denote the spatial average over "sea" pixels at instant t_m. We seek a set of spatial and temporal functions $\phi_n(\mathbf{x})$ and $a_n(t)$, so that

$$T_e(\mathbf{x},t) \approx \sum_{n=1}^{N} a_n(t_m)\phi_n(\mathbf{x}) \tag{4}$$

under the requirement that, for any N, the mean squared error over the entire set, defined as

$$\varepsilon = \sum_{m=1}^{M} \left\langle \left| T_e(\mathbf{x},t) - \sum_{n=1}^{N} a_n(t_m)\phi_n(\mathbf{x}) \right|^2 \right\rangle \tag{5}$$

is minimum. This minimisation problem leads to an eigenfunction equation of the form (Sirovich and Everson, 1992)

$$C_e\phi_k(\mathbf{x}) = \lambda_k\phi_k(\mathbf{x}) \quad k = 1\ldots N \tag{6}$$

where C_e is, up to a constant, the $N \times N$ dimension "spatial" covariance matrix. Its (i,j) element repre-

sents the covariance between the spatially demeaned SST at instants i and j.

$$C_e(i,j) = \langle T_e(\mathbf{x}, t_i) T_e(\mathbf{x}, t_j) \rangle \quad (7)$$

A set of N eigenvalues λ_k and N new eigenfunctions (or modes) $\phi_k(\mathbf{x})$ are obtained from the eigenvalue Eq. (6). The eigenfunctions $\phi_n(\mathbf{x})$ are obtained as linear combinations of the original temperature images. They form an orthonormal set:

$$\int_S \phi_i(\mathbf{x}) \phi_j(\mathbf{x}) \mathrm{d}x = A_i \delta_{ij} \quad (8)$$

where A_i is a normalization constant, and the domain S is defined over the "sea" pixels. It is this property of orthogonality what makes the EOF analysis so interesting, because each eigenfunction explains a separate part of the variance of the original set. Consequently, each eigenvalue λ_k is interpreted as the joint variance associated to all the spatial gradients observed in the original dataset that its associated eigenfunction $\phi_k(\mathbf{x})$ explains.

The finite number of images used to estimate the EOF is a limitation in the sense that not all the modes are statistically significant. Another limitation is that, if two eigenvalues are too close, an effective degeneration between eigenfunctions may take place. Following North et al. (1982), it is possible to assign an "error distance" $\delta\lambda$ to each eigenvalue λ, so that if another eigenvalue is closer than $\delta\lambda$ to the eigenvalue λ, then degeneration is likely to occur. The "error distance" $\delta\lambda$ is given by

$$\delta\lambda \approx \lambda \left(\frac{2}{N} \right)^{1/2} \quad (9)$$

where λ is the eigenvalue, $\delta\lambda$ its associated "error distance" and N the number of images used in the EOF analysis. One mode is considered significant only if the error of its associated eigenvalue λ is smaller than the distance $\Delta\lambda$ between λ and its nearest eigenvalue. As the number of images is large (325), $\delta\lambda$ is relatively small even for the largest eigenvalues, and given approximately by

$$\delta\lambda \sim 0.08\lambda \quad (10)$$

3. Results

3.1. Averaged SST and eigenvalue spectrum

The first useful output of the *spatial* EOF analysis is the spatially averaged SST series, that provides information on the simultaneous variation of surface temperature in the basin. At these spatial scales, the main source of basin-scale time variability comes from solar heating of the sea surface. The spatially averaged temperature time series is shown in Fig. 3. It varies from around 22.5 °C during summer and around 16.5 °C in winter, with a mean value of 19.6 °C. A harmonic fit gives an amplitude of 2.9 °C. The maximum temperatures are achieved during the second half of August. Important inter-annual variations are observed, mostly in summer maximum, with highest peaks during the first 3 years, 1993 to 1995.

The percentage distribution of the measured variance explained by the higher modes is shown in Fig. 4a. The first two modes explain 60% and 13% of the measured variance, respectively. The first four modes are, following the criterion given in Eq. (10), the only significant ones (Fig. 4b). They explain 80.5% of the measured variance (Table 1).

3.2. Modes description

The normalization of the eigenfunctions $\phi_k(\mathbf{x})$ is a matter of convenience. One possibility is to normalize them to unit variance, so that the temperature information is included in the temporal coefficients. Another possibility is to normalize the temporal coefficient series to unit variance:

$$\frac{1}{N} \sum_{m=1}^{N} \left(a_n(t_m)^2 - (\overline{a_n(t)})^2 \right) = 1 \quad (11)$$

where overbar denotes temporal mean, and $n = 1,\ldots N$. In this case, the temperature information is translated into the spatial eigenfunctions. This last choice has been followed, which implies that the information in the spatial maps can be interpreted as root mean square temperatures. Fig. 5 shows the temporal coefficient series, and Fig. 6 the spatial maps for the first four modes.

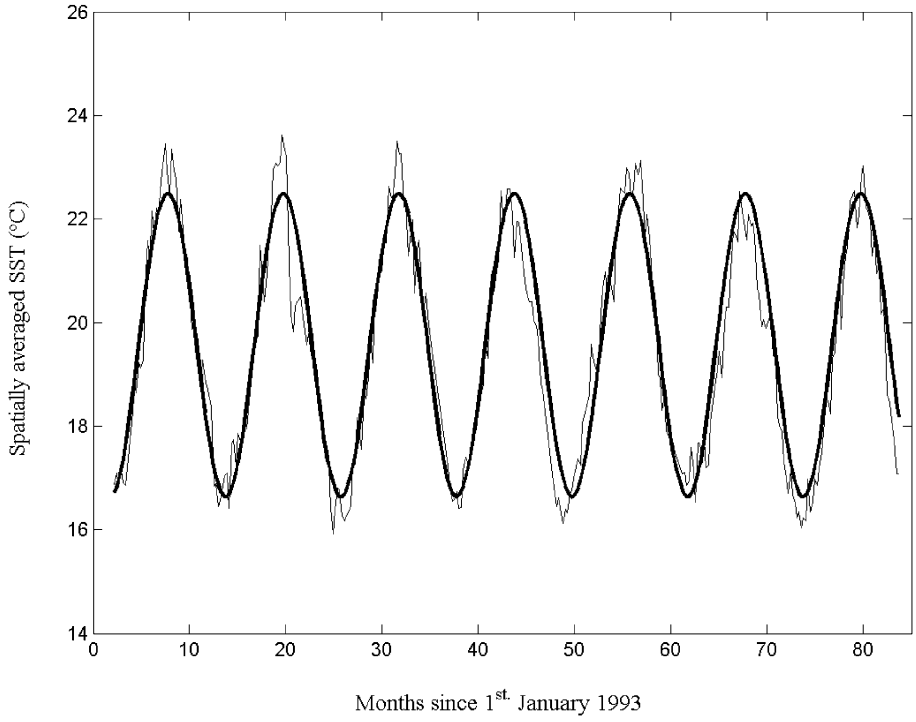

Fig. 3. Time series of the spatially averaged SST from 1993 to 1999 (thin line) and harmonic fit to a seasonal signal (thick line).

3.2.1. First mode

The first mode accounts for 60% of the measured variance. It represents, to a first approximation, a N–S temperature gradient in the basin. Since (1) this mode explains most of the spatial variance of the temperature; (2) it is also the only one with a significant non-zero mean; and (3) it has no sign changes in the temporal coefficient series, it is likely to represent the most permanent and stable thermal structures in the region. A decomposition of $a_1(t)$ into mean and fluctuating part of the form

$$a_1(t) = \overline{a_1(t)} + a_1'(t)$$

gives $\overline{a_1(t)} \simeq 1.94$. The fluctuation $a_1'(t)$ around this mean value shows a prominent annual cycle. An annual harmonic fit, $f_a^{(1)}(t) = \mathbf{A}_a^{(1)} \cdot \sin\,(\omega_a t - \alpha^{(1)})$, where $\omega_a = 365$ day^{-1} gives an amplitude $\mathbf{A}_a^{(1)} = 0.92$. The minimum is achieved at yearday 64 (beginning of March), and the maximum at yearday 246 (beginning of September). The explanation of this annual signal should be related to direct solar heating of surface waters. In fact, it is almost locked-in-phase with the annual cycle of the averaged temperature over the entire regions.

The most noticeable characteristic in the spatial map of this mode (Fig. 6a) is the nearly circular feature of warmer (than the mean) waters in the southern part of the study area. Animated sequences of the original images show clockwise advection of different temperature patterns along the periphery of a warm water core, supporting the hypothesis of a warm anti cyclonic gyre that would extend southwards, out of the study area. Fig. 6a shows that the length scale of this gyre is of the order of 200 to 300 km, which matches well the length-scale of the meandering jet in the numerical model by Johnson and Stevens (2000), suggesting that it could be the last meander of the Azores current. North of the gyre the upwelling area around Cape S. Vicente is also described by this mode. The high negative values of this mode around the Cape and the fact that the coefficients $a_1(t)$ are always positive also suggest that the upwelling is a quasi-permanent feature. The negative values extend to the east as far as

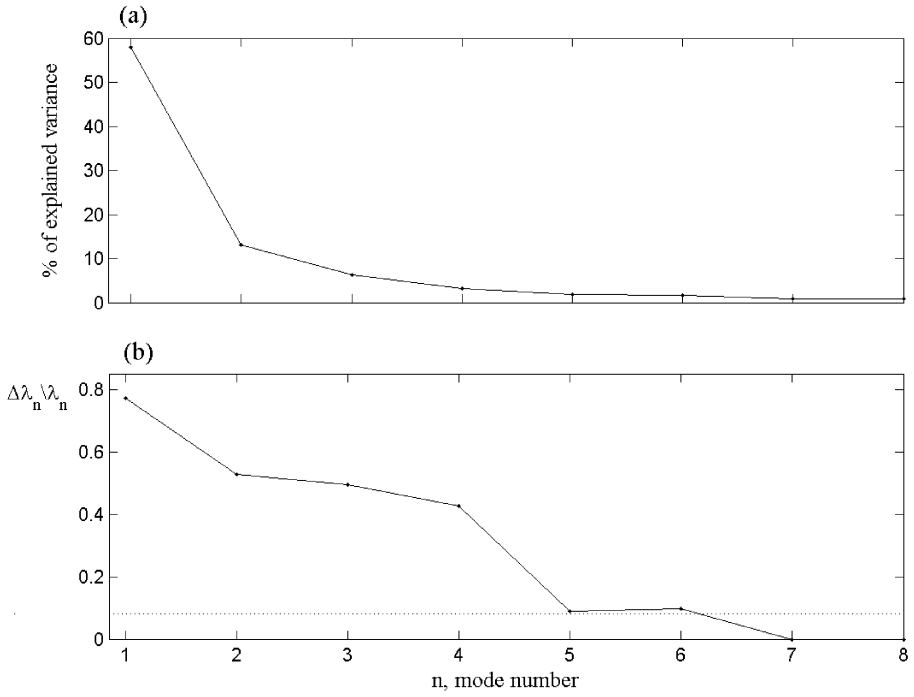

Fig. 4. (a) Percentage of variance explained by the higher modes. (b) Ratio of the minimum variance distance $\Delta\lambda$ to the corresponding eigenvalue λ_n. The dotted lines marks the condition $\delta\lambda_n = 0.08\lambda_n$.

Huelva. Some smaller-scale features are visible at the eastern end of the circular-like warm gyre. The first one is the warm tongue extending towards the Strait of Gibraltar, which appears to feed the Atlantic inflow. The second one consists in a reduced region of cold waters around Cape Trafalgar. This is a persistent thermal feature that has been related to extended vertical mixing caused by strong tidal currents flowing over a shallow rock band that runs some kilometers normal to the coast (Vargas et al., 1999). Finally there is a faint plume of warm water that seems to exit from Guadalquivir river estuary and/or from the Bay of Cádiz. The plume extends southwards, and eventually merges with the warm tongue that extends towards the Strait of Gibraltar from the center of the Gulf.

Table 1
Percentage of variance explained by the first four spatial modes

	Mode			
	1	2	3	4
Percentage of variance	58	13	6	3
Percentage of cumulative variance	58	71	77	80

3.2.2. Second mode

The temporal coefficient series of this and the following modes change sign. An area of warm temperatures in the modal map (Fig. 6b) represents a warm water area only when the temporal coefficients are positive, and cold water when they are negative. The opposite is also valid for the cold water zones in the modal spatial map. Thus, regions with opposite signs must be interpreted as if their temperatures were fluctuating 180° out-of-phase.

The second mode accounts for 13% of the measured temperature variance. It explains, to a first approximation, the east–west variability over the basin. The temporal coefficient series has approximately zero mean, and also shows a seasonal cycle (Fig. 5). A harmonic fit $f_a^{(2)}(t) = \mathbf{A}_a^{(2)}\sin(\omega_a t - \alpha^{(2)})$, gives an amplitude $\mathbf{A}_a^{(2)} = 0.95$. The maximum is achieved at yearday 7, and the minimum at yearday 187 (beginning of July). Notice, however, that this seasonal cycle is strongly anharmonic, in the sense that the amplitude is usually underestimated with the harmonic fit.

The main thermal patterns observed in the temperature map of this mode (Fig. 6b) are: (1) a warm water

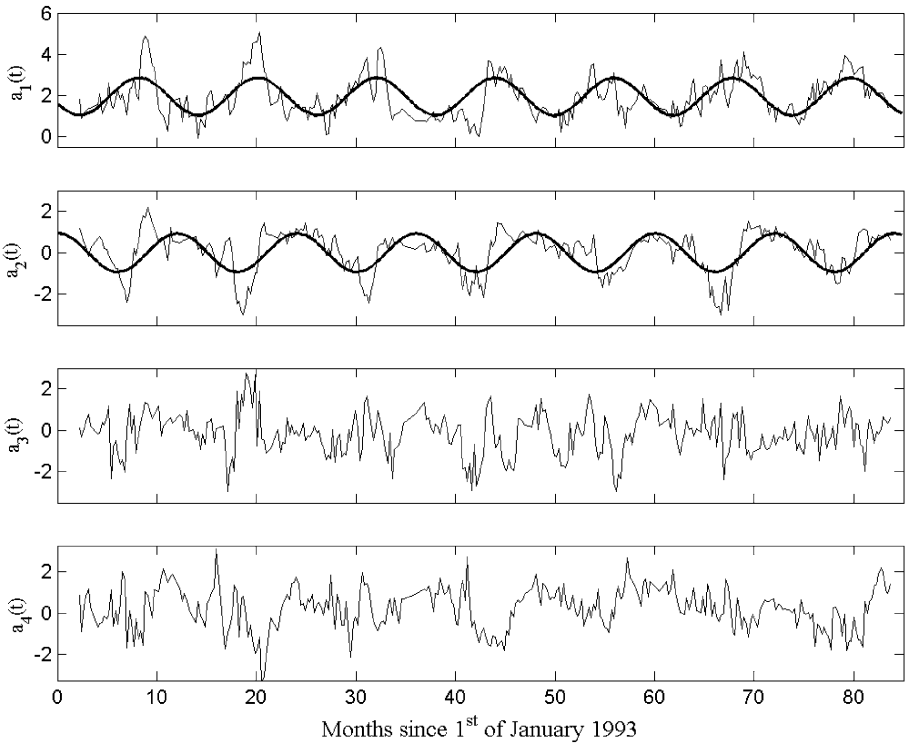

Fig. 5. Temporal coefficient series of the first four modes (thin lines). Thick lines are harmonic fits to seasonal signals for the first and second modes.

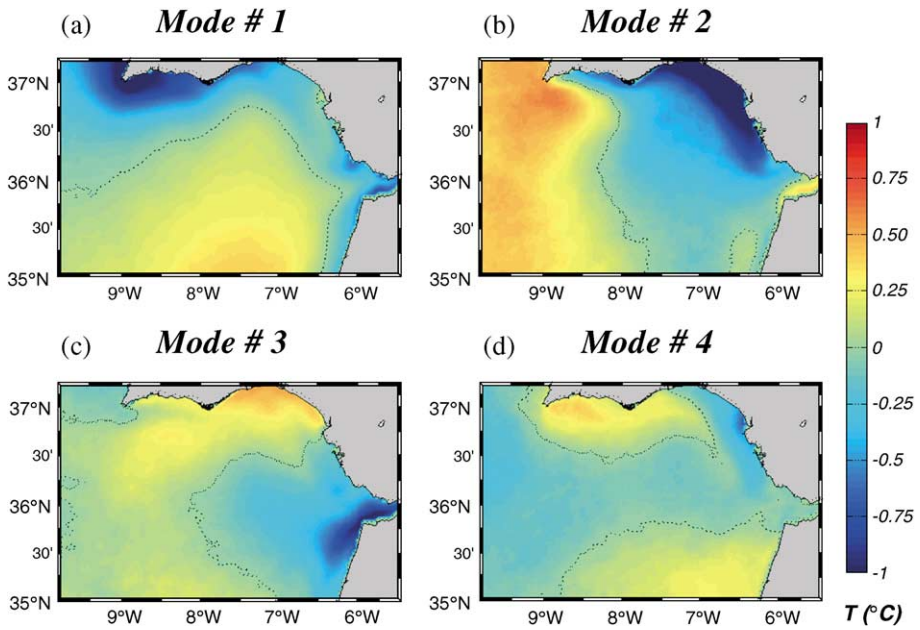

Fig. 6. Spatial maps corresponding to the first four modes.

region of intermediate intensity ($T_{rms} \simeq 0.5$ °C) in the western part of the study region; (2) a cold water region over the shelf of the Iberian coast, roughly from Cape Santa María to Cape Trafalgar. It is approximately limited by the 100–200 m isobaths, and has a maximum width of around 50 km at its central part. The highest contrast is found close the coast ($T_{rms} \simeq 2$ °C); (3) a small region of slightly warm waters, at the southern part of the Strait of Gibraltar, that extends southwards along the western coast of Morocco; and (4) a region of almost zero temperature variance at the center of the basin. Thus, this second mode describes a relative cooling of the surface waters over the Iberian shelf and a warming of the open sea waters in winter, and a quick heating of the former and a cooling of the latter in summer, following the sign changes in the temporal coefficient series. It modifies the seasonal variation described by the first mode to take into account the higher rate at which shelf waters warm and cool.

Later on it will be shown that the combination of the seasonal cycle of the first and second mode recovers the annual variation of temperature in the basin, producing a variety of new thermal features that are not evident from the separated maps of both modes.

The forcing mechanism of this mode is not clear. The seasonal periodicity indicates that this mechanism must be one with large spatio-temporal scales. It may be associated to seasonal changes in the circulation pattern of the meandering branch of the Azores current described above. Another possibility is that it may be governed by changes in the position and extension of the Azores atmospheric high. Further work is needed to allow for non-speculative arguments.

3.2.3. Third mode

The third mode explains 6% of the measured temperature variance. The temporal coefficient series, contrary to what happens with the first and second modes, has no significant seasonal variation (Fig. 5). The modal spatial map (Fig. 6c) shows high values in two regions. The first region is located off the northwestern African coast and in the Strait of Gibraltar. It has strong negative modal values. The second region is located in a relative narrow band on the shelf between Cape Santa María and the mouth of Guadalquivir river. It has positive values, so that the temperature variance induced by the third mode in this region is in opposition phase to that in the former region close to the Strait. These two zones are out of phase and recall the spatial structure of the bimodal configuration observed by Folkard et al. (1997) in summer sequences.

Fig. 7 shows the low-frequency zonal wind stress series at Tarifa (thick line), normalized to unit standard deviation and superimposed to the temporal coefficient series of the first four modes (thin lines). There is a strong visual correlation between the coefficient series of mode three and the wind stress. (The correlation coefficient is higher than 0.6). The correlation with the other modes is much lower, though it may not be rejected that, occasionally, wind may excite them. The third mode is thus identified as the principal response of the SST in the Gulf to the local wind stress, that is mainly oriented in the zonal direction (Fiúza et al., 1982; Fiúza, 1983).

Thus, the interpretation of the modal map provides with valuable information on wind-induced upwelling. Westerlies induce a moderate ($T_{rms} \simeq 0.5$ °C) upwelling in the southern Iberian coast, between Cape Santa María and Guadalquivir river estuary. A fainter, cold water plume extends southeastwards from this region. On the other hand, warm waters are accumulated in the southwestern part of the Strait of Gibraltar.

The conditions under easterlies would be just the opposite. A cold water region appears in the southwestern part of the Strait, probably due to Ekman transport induced by the strong easterlies that usually take place in the Strait. Surface waters east of Cape Santa María warms, possibly due to advection of warm waters colder shelf waters.

3.2.4. Other modes

The fourth mode (3% of variance) temporal coefficient series has also a seasonal variation, though less clear than those of the first two modes. It may represent a correction to the situation represented by the first mode. Its spatial amplitude is only important around the estuary of the Guadalquivir river.

The remaining 321 modes account for a joint temperature variance of 20%. The fifth mode (not shown) represents a warm water of circular shape of about 150 km, south of Cape Santa María, with a water tongue that extends to the Strait of Gibraltar. The sixth mode (not shown) has as unique remarkable feature a slightly

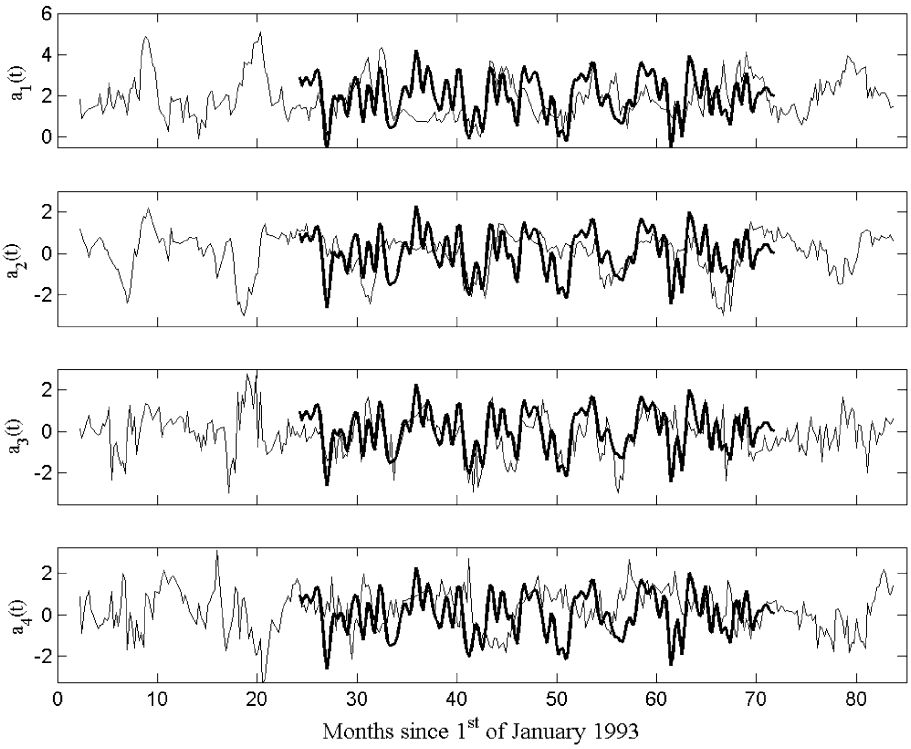

Fig. 7. Temporal coefficient series of the first four modes (thin lines). Thick lines represent normalized time series of the zonal wind at Tarifa. A suitable mean has been added to this series in each case, for better comparison with the temporal coefficient series.

high-variance region south Cape S. Vicente that extends meridionally around 200 km.

4. Synthetically generated SST sequences

4.1. The seasonal cycle

It is interesting to reconstruct the seasonal variability of the surface temperature in the basin from the most important modes (see, for example, Gazic et al., 1997, for a discussion of the seasonal variability in the Adriatic Sea). Only the first and second modes are used in the seasonal synthesis process, since they are the main contributors to seasonal variability (the small contribution of the fourth mode is neglected). The monthly reconstructed SST maps where obtained as

$$\Psi_m(\mathbf{x}) = \overline{\left(f_a^{(1)}(t)\right)}_m \phi_1(\mathbf{x}) + \overline{\left(f_a^{(2)}(t)\right)}_m \phi_2(\mathbf{x}) \qquad (12)$$

where $m = 1,2,\ldots,12$, and $\overline{(\ldots)}_m$ denotes the temporal mean over year–month m. The 12 maps derived this way (see Fig. 8) are the reconstruction of the monthly averaged annual variation of SST patterns in the basin for the time period analysed. A comparison of these maps with real SST images should be done with care, because several effects with no seasonal variability have not been taken into account in the reconstruction, so that they may strongly differ from instantaneous situations.

There are two main situations over the year. The first one dominates in wintertime, and is characterised by the presence of a large warm water core that extends more than 300 km zonally in the southern half of the basin. In the northern half, off the Iberian coast, there exists a cold water or upwelling region that extends from Cape S. Vicente to the Strait of Gibraltar. Thermal gradients are rather small everywhere. The paradigm of this situation is the map of January.

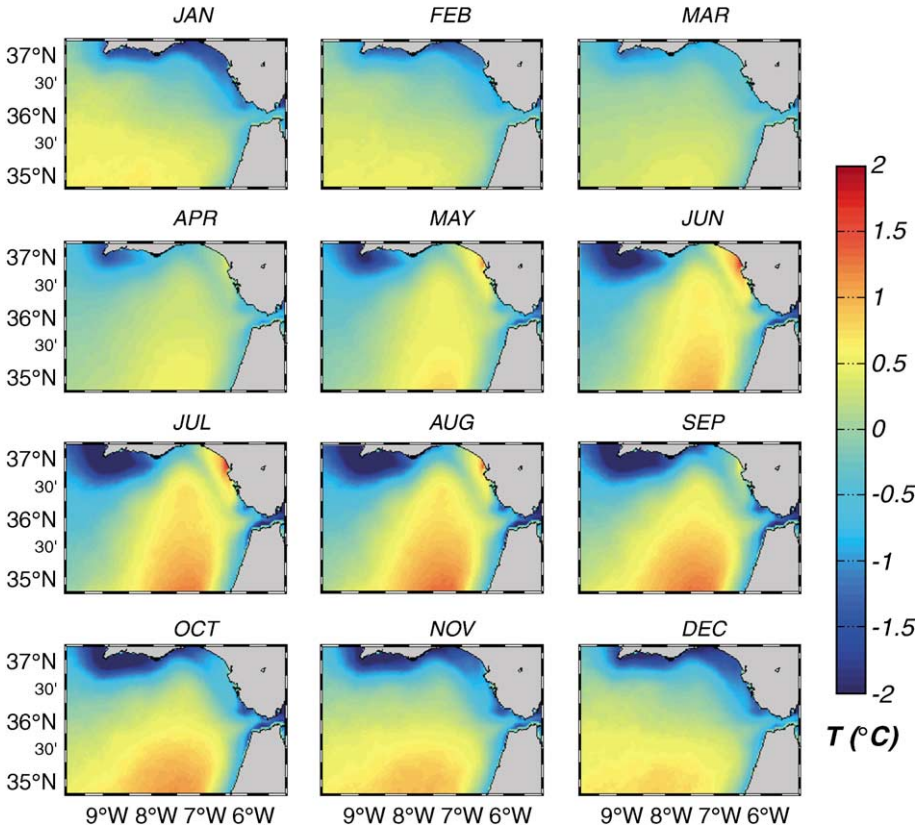

Fig. 8. Monthly reconstructed SST maps obtained from the combination of the seasonal harmonic fits of the first and second modes.

The second situation, which dominates in summertime, is characterised by a deformation of the warm core, which is stretched in the meridional direction. An example of this situation is the map of July. This stretching allows these warm waters to reach the coastal zone between Cape Santa María and the Guadalquivir river mouth. Also, the upwelling around Cape S. Vicente extends to the south, west of the gyre. An animated sequence of the images shows that, in some years, that this upwelling may extend more than 100 km. to the south off Cape S. Vicente during some weeks in late summer. Finally, a small pool of warm water is observed around the mouth of the Guadalquivir river. It does not seem to be related to the warm core waters, but rather to some kind of coastal/river process. In fact, both thermal features are well separated in the images. The evolution along the rest of the year is just the change from one of these extreme situations to the other.

Of special interest is the evolution of the surface temperature in the southwestern Iberian shelf along the year. In early winter (December–January) the upwelling area extends as far to the west as Cape Trafalgar. During the following months it suffers a setback until it is finally confined to the east of Cape Santa María from April to August. During spring and summer the shelf between Cape Santa María and Cape Trafalgar is occupied by the northern edge of the warm core and by the mentioned pool of warm water at the Guadalquivir river mouth. Finally, the upwelling area starts growing to the east in autumn, and eventually reaches Cape Trafalgar again in early winter.

4.2. An estimate of the zonal wind effect on the SST

The main response of SST to wind stress is contained in the third mode, as the correlation between the zonal wind stress at Tarifa and the coefficient time

series of this mode indicates. Thus, it is possible to sketch the wind-forced SST variation by introducing this third mode into the reconstructed spatial maps. Instead of using the map generated with Eq. (12), seasonal maps have been generated in a similar way, but with 3-month, rather than 1-month, averages. They are shown in the central column in Fig. 9, for winter, spring, summer and autumn, respectively. The modifications that easterlies (Fig. 9, right column) and westerlies (left column) produce have been obtained by adding and subtracting the third mode spatial map to each of those maps. As the temporal coefficient series has unit standard deviation, this factor would correspond to a moderately high wind stress.

Easterlies and westerlies have well-differentiated influence on the SST of the Gulf of Cádiz for all seasons. As it would be expected, the maps show similar modifications on the temperature patterns for different seasons but the same wind conditions. The main effects of westerlies are: (1) an enhancement of the warm water signature of the water tongue flowing into the Strait of Gibraltar; (2) an extension of Cape S. Vicente upwelling to the east of Cape Santa María; and (3) an enhancement of the coastal warm water pool off Guadalquivir River and Cádiz city, in spring and summer, which appears as a warm filament that merges with the above mentioned warm tongue. On the other hand, easterlies produce a strong upwelling in the area west of the Strait of Gibraltar, and a heating of the water on the shelf north of Cádiz for all seasons. Consequently, the Cape S. Vicente upwelling is less extended to the east. The anticyclonic gyre is pushed to the west and, at the same time, a small warm eddy tends to detach from its northern edge. Folkard et al. (1997) observed a similar pattern modification during summer. Specially remarkable is the similitude of their Fig. 3 with the maps in Fig. 9 in the present work, corresponding to summer conditions.

Although the relationship between zonal winds and the third mode is clear, it has been noted that other

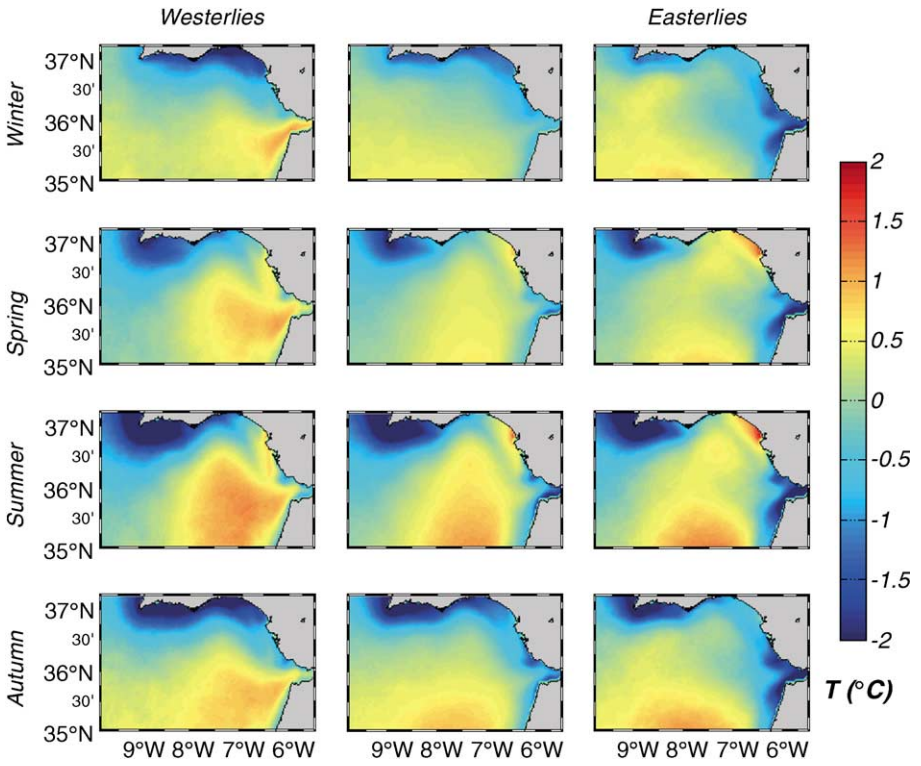

Fig. 9. From top to bottom: winter, spring, summer, and autumn mean seasonal SST maps obtained from the first and second modes (central column), and modifications of the former maps by the estimation of the effect of westerlies (left column) and easterlies (right column) winds.

modes may be accounting also for the SST response to wind conditions, not only over the Gulf itself, but at larger spatial scales. In Fiúza (1983), it is stressed that the S. Vicente upwelling, as a part of the western Portuguese coast upwelling system, is strongly affected by the meridional winds along that coast. In particular, he describes situations were northerly winds (that dominate during summer and are the responsible of the enhancement of the Portuguese upwelling during that part of the year) force upwelled waters north Cape S. Vicente to "turn around" the cape, extend eastwards along the southern coast, and to finally form a cold plume at Cape Santa María, similar to the cold plume forced by westerlies.

Wind data used in the present work do not allow to asses the influence of meridional winds, because winds at Tarifa are strongly oriented in the meridional direction by the local topography. However, we would like to stress that the negative of the spatial map corresponding to the fourth mode (Fig. 6d) shows similar features. Thus, we feel that the fourth mode can be accounting for the response of the SST to the forcing by the dominant, large-scale meridional winds. In fact, the hardly conspicuous seasonal signal in the temporal coefficient series of this mode has a negative maximum approximately in summer, consistent with northerlies winds during that part of the year. Anyway, we recognise that this is just a speculation, and needs to be further investigated.

5. Conclusions

A study of the SST variability in the Gulf of Cádiz region has been presented in this work. It is based on a set of 325 weekly averaged SST images covering a 7-year period from 1993 to 1999. The mathematical technique known as EOF Analysis has been used to compress and interpret the large amount of spatio-temporal information. The dominant "spatial" modes of the SST field have been estimated. Two modes have been found to dominate the temperature spatial variance in the area. The first one is similar to the "mean" SST structure and explains 60% of the SST variance. Its spatial map depicts a large warm waters core in the southern part of the region, and the well-known upwelling zone around Cape S. Vicente. The second mode, explaining 13% of the variance, is the main perturbation to this "mean" situation. It has a strong influence in summer, explaining the change in the shape of the warm core and the strong heating of the shelf waters between Cape Santa María and Cape Trafalgar. The main seasonal variation of the SST can be recovered from the annual signals of these two modes. It has been shown that the temperature of the shelf waters between Cape Santa María and Cape Trafalgar have a strong seasonal variation, with colder than the mean waters in autumn–winter, but warmer than the mean in spring–summer.

A third mode has been identified as the main response of the SST field to the local zonal wind, though visual inspection gives some indication that other modes may be also influenced by the wind stress. The effect of the zonal wind in the SST images has been illustrated using four situations, corresponding to the reconstructed seasonal maps by composing the first and second modes. It has been found that westerlies tend to extend the S. Vicente upwelling to the east of Cape Santa María, and they also seem to enhance the flow from the warm water core into the Strait of Gibraltar. On the contrary, easterlies produce upwelling to the west of the Strait, in both northern and southern shores (although the southern one being much stronger), and confines the S. Vicente upwelling to the west of Cape Santa María. This last situation is specially noticeable in spring and summer.

Acknowledgements

This work has been supported by the CICYT (Spanish National Program of Marine Science and Technology) MAR99 0643-C03-01 project, and by European Commission through CANIGO (MAS3-Pl95-0443) and MAGOII (MED 96 070) projects. We are grateful to the DFD, Deutsches Fernerkundungsdatenzentrum (German Remote Sensing Data Center) for providing the SST images, and to the Instituto Español de Meteorología (Spanish Meteorological Institute) for supplying the wind data. We are also grateful to Margarita Parada for her comments and bibliographic supply on EOF analysis of SST images. Figs. 1, 6, 8 and 9) were composed using the free software package m_map v1.3g for Matlab, by Rich Pawlowicz.

References

Álvarez, A., López, C., Riera, M., Hernández-García, E., Tintoré, J., 2000. Forecasting the SST space–time variability of the Alborán Sea with genetic algorithms. Geophys. Res. Lett. 27 (17), 2709–2712.

Ambar, I., Armi, L., Bower, A.S., Ferreira, T.C., 1999. Some aspects of time variability of the Mediterranean Water off south Portugal. Deep-Sea Res. 46, 1109–1136.

Baringer, M.O., Price, J.F., 1997. Mixing and spreading of the Mediterranean outflow. J. Phys. Oceanogr. 27, 1654–1677.

Bower, A.S., Armi, L., Ambar, I., 1995. Direct evidence of meddy formation off the southwestern coast of Portugal. Deep-Sea Res. 42, 1621–1630.

Bryden, H.L., Candela, J., Kinder, T.H., 1994. Exchange through the Strait of Gibraltar. Prog. Oceanogr. 33, 201–248.

Candela, J., Winant, C., Bryden, H.L., 1989. Meteorologically forced subinertial flows through the Strait of Gibraltar. J. Geophys. Res. 94, 12667–12674.

Echevarría, F., García-Lafuente, J., Bruno, M., Gorsky, G., Goutx, M., González, N., García, C.M., Gómez, F., Vargas, J.M., Picheral, M., Striby, L., Varela, M., Alonso, J.J., Reul, A., Cózar, A., Prieto, L., Sarhan, T., Plaza, F., Jiménez-Gómez, F., 2002. Physical–biological coupling in the Strait of Gibraltar. Deep-Sea Res. II 49, 4115–4130.

Everson, R., Sirovich, L., 1995. The Karhunen–Loève transform for incomplete data. J. Opt. Soc. Am. Ser. A 12 (8), 1657–1664.

Everson, R., Cornillon, P., Sirovich, L., Webber, A., 1997. An empirical eigenfunction analysis of the sea surface temperature in the western North Atlantic. J. Phys. Oceanogr. 27, 469–479.

Fang, W., Hsieh, W.W., 1993. Summer sea surface temperature variability off Vancouver Island from satellite data. J. Geophys. Res. 98, 14391–14400.

Fiúza, A.F.G., 1983. Upwelling patterns off Portugal. In: Suess, E., Thiede, J. (Eds.), Coastal Upwelling. Plenum, New York, pp. 85–98.

Fiúza, A.F.G., de Macedo, M.E., Guerreiro, M.R., 1982. Climatological space and time variations of the Portuguese coastal upwelling. Oceanol. Acta 5, 31–40.

Folkard, A.M., Davies, P.A., Fiúza, A.F.G., Ambar, I., 1997. Remotely sensed sea surface thermal patterns in the Gulf of Cadiz and the Strait of Gibraltar: variability, correlations, and relationships with the surface wind field. J. Geophys. Res. 102, 5669–5683.

García, C.M., Prieto, L., Vargas, M., Echeverría, F., García-Lafuente, J., Ruiz, J., Rubin, J.P., in preparation. Hydrodynamics and the spatial distribution of planckton and TEP in the Gulf of Cádiz (SW Iberian Peninsula).

García-Lafuente, J., Vargas, J.M., Plaza, F., Sarhan, T., Candela, J., Bascheck, B., 2000. Tide at the eastern section of the Strait of Gibraltar. J. Geophys. Res. 105 (C6), 14197–14213.

García-Lafuente, J., Delgado, J., Vargas, J.M., Vargas, M., Plaza, F., Sarhan, T., 2002. Low-frequency variability of the exchanged flows through the Strait of Gibraltar during CANIGO. Deep-Sea Res. II 49, 4051–4067.

Gazic, M., Marullo, S., Santoleri, R., Bergamasco, A., 1997. Analysis of the seasonal and interannual variability of the sea surface temperature field in the Adriatic Sea from AVHRR data (1984–1992). J. Geophys. Res. 102, 22937–22946.

Hernández-Guerra, A., Nykjaer, L., 1997. Sea surface variability off north-west Africa: 1981–1989. Int. J. Remote Sens. 18, 2539–2558.

Johnson, J., Stevens, I., 2000. A fine resolution model of the eastern North Atlantic between the Azores, the Canary Islands and the Gibraltar Strait. Deep-Sea Res., I 47, 875–899.

Lacombe, H., Richez, C., 1982. The regime of the Strait of Gibraltar. In: Nihoul, J.C.J. (Ed.), Hydrodynamics of Semi-Enclosed Seas. Elsevier, Armsterdam, pp. 13–73.

Lagerloef, G.S., Bernstein, R.L., 1988. Empirical orthogonal analysis of advanced very high resolution radiometer surface temperature patterns in Santa Barbara Channel. J. Geophys. Res. 93, 6863–6873.

Lorenz, E.N., 1956. Empirical orthogonal functions and statistical weather prediction. Sci. Rep. No. 1, Statist. Forecasting Proj., Dept. Meteor., MIT, 49 pp.

North, G.R., Bell, T.L., Cahalan, R.F., Moeng, F.J., 1982. Sampling errors in the estimation of empirical orthogonal functions. Mon. Weather Rev. 110, 699–706.

Obukhov, A.M., 1947. Statistically homogeneous fields on a sphere. Usp. Mat. Nauk 2, 196–198.

Ochoa, J., Bray, N.A., 1991. Water mass exchange in the Gulf of Cadiz. Deep-Sea Res. 38 (Suppl. 1), 465–503.

Parada, M., Cantón, M., 1998. Sea surface temperature variability in Alborán sea from satellite data. Int. J. Remote Sens. 19, 2439–2450.

Reul, A., Vargas, J.M., Jiménez-Gómez, F., Echevarría, F., García-Lafuente, J., Rodríguez, J., 2002. Exchange of planktonic biomass through the Strait of Gibraltar in late summer conditions. Deep-Sea Res. II 49, 4131–4144.

Rubín, J.P., Cano, N., Preto, L., García, C.M., Ruiz, J., Echevarría, F., Corzo, A., Gálvez, J.A., Lozano, F., Alonso-Santos, J.C., Escáñez, J., Juarez, A., Zabala, L., Hernández, F., García Lafuente, J., Vargas, M., 1999. La estructura del ecosistema pelágico en relación con las condiciones oceanográficas y topográficas en el golfo de Cádiz, estrecho de Gibraltar y mar de Alborán (sector Noroeste) en Julio de 1995. Inf. Téc.-Inst. Esp. Oceanogr. 175. 73 pp.

Sirovich, L., Everson, R., 1992. Analysis and management of large scientific databases. Int. J. Supercomput. Appl. 6, 50–68.

Stevenson, R.E., 1977. Huelva front and Málaga, Spain, Eddy Chain as defined by Satellite and Oceanographic Data. Dtsch. Hydrogr. Z. 30 (2), 51–53.

Vargas, M., Sarhan, T., Lafuente, J.G., Cano, N., 1999. An advection–diffusion model to explain thermal surface anomalies off Cape Trafalgar. Bol. Inst. Esp. Oceanogr. 15 (1–4), 91–99.